Observations of exchange between the South China Sea and the Sulu Sea

Janet Sprintall,[1] Arnold L. Gordon,[2] Pierre Flament,[3] and Cesar L. Villanoy[4]

Received 20 September 2011; revised 12 March 2012; accepted 26 March 2012; published 24 May 2012.

[1] The velocity and transport, with thermohaline properties, are determined from simultaneous moored time series within Mindoro, Tablas and Panay Straits that connect the South China Sea (SCS) and Sibuyan Sea to the Sulu Sea. These passages provide the only pathway for the SCS throughflow below thermocline depths and play a critical role in regulating the heat and freshwater balance within the Philippine archipelago. The upper layer in Mindoro Strait has a distinctly seasonal cycle with northward flow during the boreal summer southwest monsoon and southward flow during the winter northeast monsoon. In contrast, upper layer flow in Panay and Tablas Straits is intraseasonal. Extraordinarily strong pulses that begin at intermediate depth in the fall transition and shoal toward the sub-thermocline during the northeast monsoon are found in Mindoro and Panay Straits. These southward flows are strongly correlated to the SCS large-scale circulation and remote wind-forcing off Vietnam. Temperature and salinity in Mindoro support the SCS source of this Subtropical Water. Southward benthic flow in Mindoro and Panay act to ventilate the deeper Sulu Sea. Bottom temperatures suggest the cooler Mindoro overflow mixes with the warmer benthic waters from Tablas before exiting Panay Strait into the Sulu Sea. The 2008 mean annual total-depth transports were very small, O(0.1 Sv), although individual transport estimates of 1–2 Sv were observed in all depth layers over the year. The mooring deployment coincided with a strong La Niña when the Pacific inflow into the SCS is expected to be weaker, and subsequently transports are lower.

Citation: Sprintall, J., A. L. Gordon, P. Flament, and C. L. Villanoy (2012), Observations of exchange between the South China Sea and the Sulu Sea, *J. Geophys. Res.*, *117*, C05036, doi:10.1029/2011JC007610.

1. Introduction

[2] The Philippine archipelago is an oceanographically unique environment with a varied and complex ocean bathymetry and island configuration that affects the variable circulation and regional dynamics (Figure 1). The processes governing variability within the Philippine seas occur over a range of spatial and temporal scales. On the large scale, there is exchange of mass and properties between the internal Philippine seas and the bounding western Pacific Ocean and South China Sea (SCS). This exchange may be modulated over various time scales, for example by episodic remote forcing of large-scale planetary Rossby waves from the western Pacific Ocean that can penetrate into the internal seas [*White et al.*, 2003; *McClean et al.*, 2005], or by regional forcing on intraseasonal, seasonal and interannual time scales related to the monsoonal reversing winds [*Han et al.*, 2008] and ENSO. Monsoon surge events cause intensified wind jets through the gaps along the mountainous topography of many Philippine islands, creating strong wind curl patterns in their lee that induce oceanic eddy shedding [*Pullen et al.*, 2008, 2011; *May et al.*, 2011]. On smaller space and shorter time scales, the narrow straits and the abrupt changes in bathymetry within and between the Philippine basins can often result in swift tidal currents [*Logutov*, 2008; *Lermusiaux et al.*, 2011; *Jones et al.*, 2011]. Hydraulically controlled benthic overflows can cause turbulence that leads to elevated mixing [*Tessler et al.*, 2010], with important consequences to the ventilation of the many deep basins within the Philippine archipelago, impacting their geochemistry and regional primary productivity [*Gamo et al.*, 2007; *Takeda et al.*, 2007].

[3] Flow through Luzon Strait (sill depth 2200 m), between Taiwan and Luzon island in the northern Philippines, enters the SCS from the western Pacific Ocean. The SCS is connected to the deep Sulu Sea basin (~5000 m), west of the main Philippine archipelago, through the Mindoro Strait (~500 m) – Panay Strait (~580 m) complex to the east of the

[1]Scripps Institution of Oceanography, University of California, San Diego, La Jolla, California, USA.
[2]Lamont-Doherty Earth Observatory, Columbia University, Palisades, New York, USA.
[3]Department of Oceanography, SOEST, University of Hawai'i at Mānoa, Honolulu, Hawaii, USA.
[4]Marine Science Institute, University of the Philippines, Quezon City, Philippines.

Corresponding author: J. Sprintall, Scripps Institution of Oceanography, University of California, San Diego, 9500 Gilman Dr., La Jolla, CA 92093-0230, USA. (jsprintall@ucsd.edu)

0148-0227/12/2011JC007610

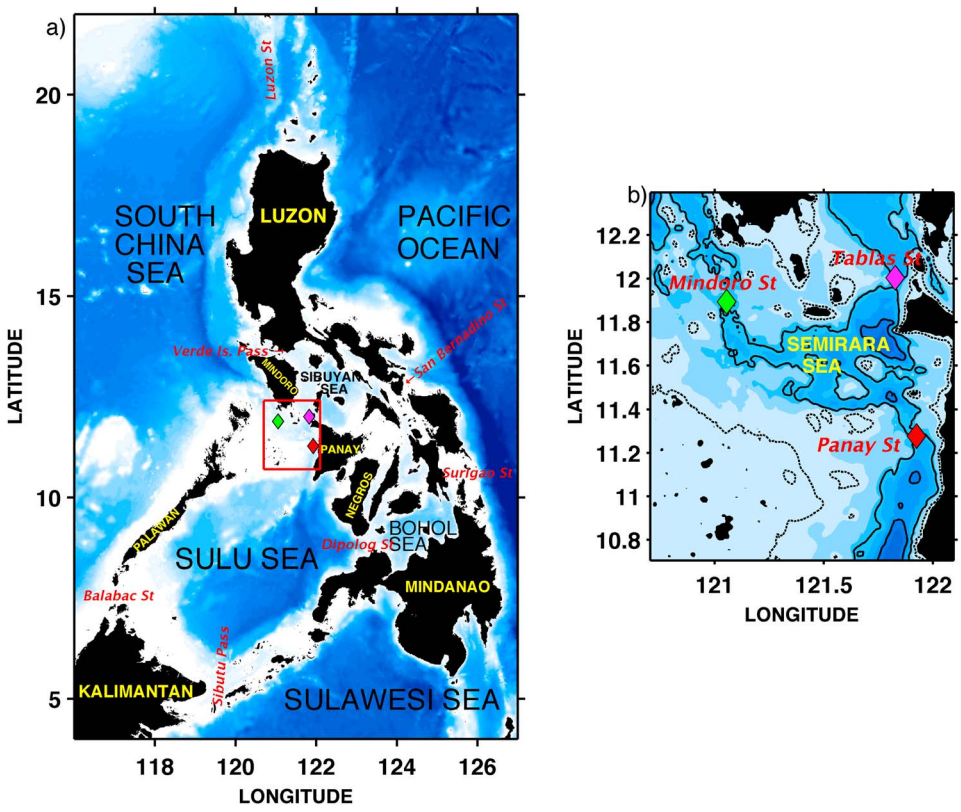

Figure 1. (a) Topography of the Philippine archipelago showing the major straits and basins. The red inset shows (b) the location of the moorings deployed during PhilEx: Mindoro (green diamond), Tablas (pink diamond) and Panay (red diamond). The 100 m (dashed), and 500 m and 1000 m (both solid) isobaths are marked in Figure 1b.

Palawan island chain (Figure 1). Mindoro Strait is the only pathway for the SCS throughflow at thermocline and sub-thermocline depth, and is thought to play a critical role in regulating the heat and freshwater balance of the SCS throughflow system [*Qu et al.*, 2006; *Fang et al.*, 2009]. The relatively narrower Balabac Strait (~10–30 m) to the west of Palawan and the wider shelf of the southwest SCS that leads to the Karimata Strait provide shallower pathways for the SCS throughflow. Waters from the western Pacific Ocean can also flow directly into the Philippine archipelago via the San Bernardino (80 m) and Surigao (~60 m) Straits (Figure 1). West of San Bernardino, waters in the Sibuyan Sea are connected to the SCS via Verde Island Passage (<100 m), and to the Sulu Sea via the Tablas Strait (~560 m) that is separated from the Mindoro-Panay Strait complex by a small basin (~1300 m) known as the Semirara Sea (Figure 1). West of Surigao, waters in the Bohol Sea are directly connected to the Sulu Sea via the Dipolog Strait (~450 m). The southern boundary of the Sulu Sea is open to the Sulawesi Sea through the Sibutu Passage (~270 m), where water can either return to the western Pacific Ocean or contribute to the Indonesian Throughflow [*Metzger and Hurlburt*, 1996].

[4] Many details of the local dynamics and circulation in the straits of the Philippine seas are still not well understood. To date, most of our knowledge of the generation, evolution and fate of the properties and flow structures within the Philippine seas has come principally from models, which have been poorly constrained by the few observational data in the region. Until recently there existed only a few discrete hydrographic surveys [e.g., *Quadfasel et al.*, 1990] and ship drift records [*Wyrtki*, 1961] that documented the circulation and properties within the region. *Wyrtki* [1961] described the surface circulation in the Sulu Sea as reversing in response to the monsoon winds. The ship-drift data suggested that during the peak of the Northeast Monsoon (NEM: December–March), Pacific Ocean surface waters enter westward through the Surigao and San Bernardino Straits into the Sulu Sea, and exit northward through Mindoro into the SCS and southward through Sibutu Passage into the Sulawesi Sea [*Wyrtki*, 1961]. During the Southwest Monsoon (SWM: June–September) the surface flow is southward from the SCS in Mindoro Strait, and circulation within the Sulu Sea is cyclonic [*Wyrtki*, 1961]. Recent high-resolution modeling studies [*Han et al.*, 2008] and remotely sensed data [*Cai et al.*, 2009] confirmed the reversing surface circulation in the Sulu Sea is mainly driven by local monsoon wind, although remote forcing can significantly modify the surface circulation and becomes more important just before the monsoon peaks. At intermediate depths, one-time hydrographic CTD surveys suggest that Subtropical Lower Water, characterized by a salinity maximum at ~200 m depth, spreads from the SCS into the Sulu Sea via Mindoro Strait [*Quadfasel et al.*, 1990; *Chen et al.*, 2006]. However, only the upper portion of North Pacific Intermediate Water (NPIW), found at depths

Table 1. The Deployment and Recovery Dates, Location, Passage Width and Depths of the PhilEx Moorings

Mooring	Deployment Date (GMT)	Recovery Date (GMT)	Location	Passage Width (km)[a]	Depth[b]
Mindoro	21 Dec 2007	19 Mar 2009	121°03.282′E, 11°53.698′N	34	460 m
Panay	7 June 2007, 5 Dec 2007	5 Dec 2007, 16 Mar 2009	121°55.464′E, 11°16.74′N	36	580 m
Tablas	3 Dec 2007	16 Mar 2009	121°49.608′E, 12°00.288′N	37	560 m

[a]Determined between the 100 m isobaths on either side of mooring using combined *Becker et al.* [2009] and PhilEx cruise multibeam bathymetry.
[b]Depth at mooring location determined using PhilEx cruise multibeam bathymetry.

of 400–800 m in the SCS, is able to pass over the 450 m sill at Mindoro Strait into the Sulu Sea. NPIW is characterized by salinity and oxygen minima [*Quadfasel et al.*, 1990]. Recent evidence shows overflow of NPIW at Panay Strait is hydraulically controlled [*Tessler et al.*, 2010], and is the primary source for the intermediate waters of the Sulu Sea [*Quadfasel et al.*, 1990; *Chen et al.*, 2006; *Tessler et al.*, 2010]. Most of the reported transport estimates in the straits of the Philippine archipelago have been based on model output. In Mindoro Strait, the models mostly estimate a mean southward transport ranging from ∼0.5 Sv to 4 Sv [*Metzger and Hurlburt*, 1996; *Lebedev and Yaremchuk*, 2000; *Fang et al.*, 2005, 2009; *Qu et al.*, 2006; *Hurlburt et al.*, 2011], with a similar range of model transport estimates reported for the outflow at the Sibutu Passage. *Qu and Song* [2009] estimate 2.4 Sv southward transport in Mindoro Strait through application of hydraulic control theory to remotely sensed altimetric and ocean bottom pressure measurements, and a 2.8 Sv Sibutu Passage outflow, suggesting a small contribution to the Sulu Sea probably enters via Dipolog Strait.

[5] Here we describe the property, velocity and transport estimates from the first moored time series measurements in Mindoro, Tablas, and Panay Straits that connect the SCS to the Sulu Sea in the Philippine archipelago (Figure 1). Mooring measurements were made as part of the Office of Naval Research "Characterization and Modeling of Archipelago Strait Dynamics," commonly referred to as the Philippine Straits Dynamics Experiment (PhilEx) [*Gordon and Villanoy*, 2011]. Along with the mooring time series, the fieldwork component of PhilEx consisted of numerous CTD and Lowered Acoustic Doppler Current Profiler (L-ADCP) measurements, glider and drifter surveys, and a high-frequency (HF) radar system installed on the island of Panay (Figure 1). Results from both the hydrographic fieldwork and modeling analyses are discussed in a special volume [see *Gordon and Villanoy*, 2011]. As part of this special volume, some of the moored velocity time series at discrete depths are presented and discussed in *Gordon et al.* [2011], in relation to a wind-driven reversal during February 2008 in *Pullen et al.* [2011], and compared to HYCOM model output in *Hurlburt et al.* [2011]. The deep overflow observed in Panay Strait is the subject of *Tessler et al.* [2010]. In this paper, our focus is the variation of the flow structure and property profiles in Mindoro, Tablas and Panay Straits. We also derive the mean and variability of the transport estimates in the straits, and discuss how they relate to the large-scale monsoonal forcing.

[6] The paper is organized as follows. In section 2 we detail the deployments and instrumentation of the PhilEx moorings. Section 3 describes the vertical structure of the velocity and property variability, and the subsequent supply of different water masses into and out of the Sulu Sea. In section 4, we first discuss the inherent assumptions behind the transport calculation for each strait, and then present the seasonal variations and means of the transport estimates. A discussion of possible forcing mechanisms is given in section 5, followed by conclusions in section 6.

2. The PhilEx Mooring Measurements

[7] The location, deployment depth, and deployment periods for the PhilEx moorings are given in Table 1. All moorings were deployed within 1–2 km of the sill in each strait as surveyed by the shipboard multibeam echo sounder. Mooring velocity instrumentation configuration was similar on all moorings (see Figure 2), with ADCPs deployed to resolve the vertical profile of the flow. The ADCPs included pressure and temperature sensors, and if there was additional mooring line available, discrete temperature-pressure and/or temperature-salinity-pressure sensors were also deployed (Figure 2). Sampling rates were set to resolve the tides, and were 30 min for the ADCPs and 15 min for the temperature and salinity sensors.

[8] The first PhilEx mooring in Panay Strait was deployed as part of the Exploratory Cruise on the *R/V Melville* in June 2007. This mooring was recovered and redeployed after 3 weeks to provide contextual data for the hydrographic measurements made as part of this cruise. Additional moorings were deployed in Mindoro Strait and in Tablas Strait during a December 2007 cruise, when the Panay mooring was recovered, refurbished and then redeployed. All moorings were recovered in March 2009.

[9] The majority of the ADCP instrumentation successfully returned 100% of the 15–18 month velocity time series record. However, as with many moorings that are deployed within the dynamic environment of narrow straits with swift tidal currents, the PhilEx moorings experienced some data loss through mooring and instrumental failure. Unfortunately, in Tablas Strait the ADCP designed to capture the bottom flows flooded at some stage during the deployment period, and efforts by a commercial data recovery service were unable to extract any information from the ADCP data card. In addition, due to surface reflection contamination, the ADCPs are often unable to sample the near-surface layer (Figure 2). For Mindoro and Tablas Straits, where the ADCPs were mounted on the moorings at 150-m and 200-m depth respectively (Figure 2), typically only the upper 20 m velocities are missing. In Panay Strait, where the ADCP was bottom-mounted, the upper 40 m of the water column is missing. In section 4, we will discuss how these data gaps are handled for the transport calculations that require full-depth velocity measurements.

[10] Pressure time series from the ADCPs and some available discrete CTD sensors were used to account for mooring blowover through tidal and low frequency forcing,

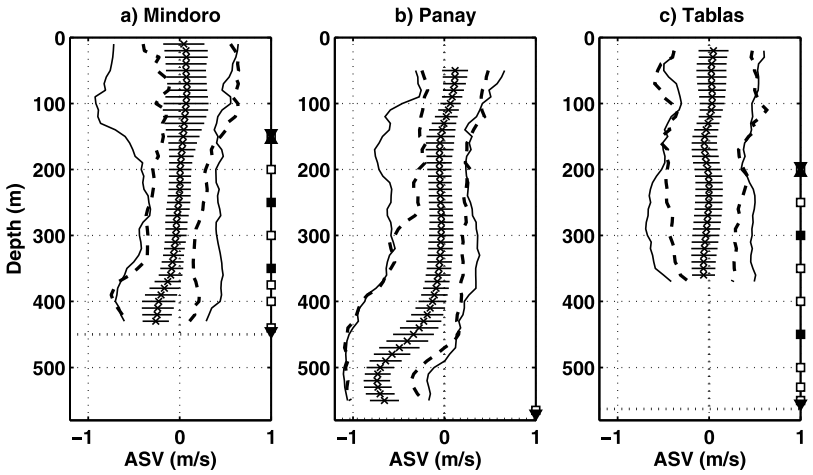

Figure 2. The 2008 mean (cross), standard deviation (black horizontal line), and range of along-strait velocity (ASV in m s^{-1}) during the Northeast Monsoon (December–March: black vertical line) and Southwest Monsoon (June–September: dashed vertical line) for the depths resolved by the ADCP measurements in (a) Mindoro, (b) Panay, and (c) Tablas Straits. Dotted line indicates the water depth at each deployment location. The location of the mooring instruments are indicated on the right-hand side of each panel: ADCP (solid triangle), temperature-pressure sensors (square); and temperature-conductivity-pressure sensors (solid square). Note that the ADCP deployed at the bottom of the Tablas mooring failed and did not return any velocity data.

although corrections to depth from mooring blowover was typically <20 m. The velocity data were then vertically linearly interpolated onto a 10-m depth grid and a common time base of 1 h. The resulting velocity time series were low-pass filtered with a 4-day Hamming window to suppress the inertial and tidal variability, and then subsampled to daily values. Finally, the Cartesian velocities in each strait were rotated into along-strait velocities (ASV) based on the orientation of the strait and the subsequent major axis of the strongest flow (typically near-bottom): Mindoro Strait 355°T (true); Tablas Strait 10°T; Panay Strait 320°T. The sign convention for ASV and transport to be used in this paper is negative (positive) toward (away from) the Sulu Sea. In most cases the cross-strait velocities (XSV) are near-zero. However, because the rotation is based mainly on the bottom flows in narrow sill channels, XSV can at times be significant in the upper layer where the channel is wider, and also where side channels may feed cross flow into the strait. Instances where XSV may contribute to the throughflow are discussed in the text.

3. Velocity and Property Variability

[11] While the primary focus of this analysis is on the distribution and variability of transport with depth in the passages leading into the Sulu Sea, it is instructive to first examine the vertical profile of ASV from the ADCP mooring data. It is the vertical distribution of the flow through each strait that, to a large extent, will set the heat flux of the flow into the Sulu Sea. Unfortunately, due to the substantial fishing and shipping pressures in these narrow passages, none of the moorings completely measured the full depth property variability, so we are unable to estimate the property transports from the available data. Nonetheless, all moorings measured bottom temperature where strong, deep overflows occur. In addition, the CTD sensors at intermediate depths on the Mindoro and Tablas moorings (Figure 2) enable us to examine the spreading of water masses from the SCS into the internal seas of the archipelago, and their relationship with the flow variability. For the interested reader, time series of the flow in each passage at depths of 150 m, 300 m and the near bottom are found in *Gordon et al.* [2011], and the full depth velocity time series of Mindoro Strait is given in *Hurlburt et al.* [2011], and of Panay Strait in *Tessler et al.* [2010].

3.1. Mean Along-Strait Velocity

[12] Figure 2 shows the mean, standard deviation, and range of ASV during the NEM and SWM for the depths resolved by the ADCP measurements in each passage for calendar year 2008, the common deployment period for each mooring (Table 1). In 2008, northward flow in the upper layer of Mindoro Strait begins in the boreal spring transition in April and continues through the SWM until the end of the fall transition in November (see Figure 4 of *Hurlburt et al.* [2011]). During the NEM, the ASV is primarily southward with strong speeds of up to ~0.9 m s^{-1} possible at 100–130 m depth (Figure 2a), although there are episodic bursts of weak or northward flow every 20 days or so [*Hurlburt et al.*, 2011]. Subsequently, the mean annual flow in the upper layer of Mindoro Strait is slightly northward at 0.1 m s^{-1} and the variability in this layer is strong (Figure 2a). Note that the near surface flow in Mindoro Strait during 2008 is of the opposite sense to that suggested by *Wyrtki* [1961], based on the expected Ekman response to the monsoonal reversals. Possible reasons for this discrepancy will be discussed below in section 5. At intermediate depths, the mean ASV in Mindoro Strait is slightly southward and the variability relatively low (Figure 2a). The southward ASV strengthens in the benthic layer, with mean speeds of ~−0.3 m s^{-1} and

maximum speeds of >0.7 m s^{-1} are possible during both the NEM and SWM (Figure 2a). While the mean XSV in Mindoro Strait is mostly negligible, in the upper layer above ~80 m there is a mean ~0.2 m s^{-1} westward flow (not shown). This relatively shallow westward XSV likely derives from Tablas Strait in response to the strong episodic northerly wind surges during the NEM [*Pullen et al.*, 2011].

[13] Similar to Mindoro Strait, the ASV in the upper layer of Panay Strait is ~0.2 ms^{-1} northward in the mean (Figure 2b). The missing ASV in the upper 40 m at this mooring site makes the connection of the near-surface flow to the monsoon variability more problematic. At intermediate depths the mean flow is slightly southward but maximum speeds of >0.6 m s^{-1} are observed, particularly during the fall transition and NEM (Figure 2b). In Panay Strait, the strong benthic overflow can reach speeds >1 m s^{-1} in either monsoon phase, with a mean of −0.7 m s^{-1} toward the Sulu Sea occurring at 520-m depth, which is 40–50 m above the bottom. The variability in the benthic layer ASV is low, and below 490 m the flow is always toward the Sulu Sea (Figure 2b). Note that the mean flow recorded in the benthic layer at the Panay Strait mooring site is stronger than that found in the (shallower) benthic layer at the Mindoro Strait mooring site. Since Mindoro Strait is the main portal for flow from the SCS into Panay Strait, this possibly implies that 1) the Mindoro mooring site may not have been optimally located to capture the strongest benthic flow through this channel; 2) the channel geometry is wider in Mindoro Strait at depth so that it can carry more flow/transport, and/or 3) there may be a significant contribution from the (not measured) benthic flow through Tablas Strait (Figure 2c) into Panay Strait. These issues will be addressed when calculations of the transports in each strait are made in section 4. The mean XSV was relatively large in the Panay Strait benthic layer, although still significantly smaller that the ASV. This is likely due to the deepening of the channel's southern bank or tidal friction [*Tessler et al.*, 2010].

[14] The mean ASV measured in the upper and intermediate depths in Tablas Strait is very weak (Figure 2c). The mean ASV alternates from slightly northward in the upper layer, southward from 140–200 m depth, near-zero at 200–270 m, then slightly southward below this to the deepest level of our ADCP mooring observations at 360 m (recall that the up-ward looking, bottom-mounted ADCP in Tablas Strait failed). While in the upper layer current speeds of equal strength can occur during either monsoon phase, at intermediate depth both northward and southward currents are stronger during the NEM compared to the SWM (Figure 2c).

3.2. Property Variability

[15] Subtropical Lower Water (also known as North Pacific Subtropical Water [*Yu et al.*, 2008; *Gordon et al.*, 2011]), characterized by a salinity maximum near ~200 m, enters the SCS via the Luzon Strait from the Philippine Sea in the Western Pacific [*Wyrtki*, 1961; *Qu et al.*, 2000]. Since the salinity maximum layer lies well above the sill depths in Mindoro and Panay Straits, this water mass is also present within the Sulu Sea basin [*Quadfasel et al.*, 1990; *Chen et al.*, 2006; *Gamo et al.*, 2007]. Two CTD sensors on the mooring in Mindoro Strait – one at a mean depth level of 206 m and another at 312 m – capture the seasonal variability in the potential temperature (θ) and salinity (S) properties of the Subtropical Lower Water (Figure 3a). Although most Sulu Sea hydrographic surveys suggest the salinity maximum occurs at ~200 m, a depth similar to where it is found in the SCS [*Qu et al.*, 2000], the Mindoro Strait time series shows the water column is slightly saltier at ~300 m compared to ~200 m (Figure 3).

[16] At 206 m, the Mindoro Strait θ-S properties are saltier and warmer when flow is toward the Sulu Sea (Figure 3a) primarily during the NEM and in the fall transition (Figure 3b). During the spring transition and SWM, the properties at 206 m in Mindoro Strait are fresher and cooler (Figure 3b) when flow is weak or northward (Figure 3a). Although there is little correspondence of temperature and salinity with flow strength and direction at 244 m depth in Tablas Strait (Figure 3a), a similar salinity range is found to that at 206 m in Mindoro Strait during the spring transition and SWM (Figure 3b). *Gordon et al.* [2011] found interleaving of the Subtropical Lower Water salinity maximum water with the shallower salinity minimum waters within the Semirara Sea that separates the two straits (Figure 1b) occurs during the spring and weakens as the SWM evolves. This suggests that the Semirara Sea is the likely source of the fresher waters in both Mindoro and Tablas Straits during these seasons (Figure 3b). In contrast, the θ-S properties at 312 m depth in Mindoro and 345 m depth in Tablas Strait show little seasonal influence (Figure 3b). There is a suggestion of slightly saltier properties at both Mindoro and Tablas with flow away from the Sulu Sea at these depths (Figure 3a). In Tablas Strait, the mean salinity is ~34.51 psu at both 244 m and 345 m depth, slightly less than the salinity maxima measured in Mindoro Strait at 207 m (~34.53) and 312 m (34.57) which has a more direct connection to the SCS. This is consistent with *Qu* [2000] who found a climatological mean salinity of ~34.54 in the salinity maximum layer of the southern SCS near Mindoro Strait. The lower salinity in Tablas Strait may also be a consequence of mixing with lower salinity water masses from within the Sibuyan Sea [*Gordon et al.*, 2011].

[17] The ventilation of the Sulu Sea is known to occur through strong benthic currents that spill over the sills in the Mindoro-Panay Strait complex [*Quadfasel et al.*, 1990; *Tessler et al.*, 2010]. As noted above, the primary source water is NPIW, which is characterized by a low salinity and low oxygen core, found at depth levels of approximately 400–500 m in the SCS [*Qu et al.*, 2000; *Tessler et al.*, 2010]. Hydrographic surveys suggest a θ of ~9.8°C in Mindoro Strait that is much warmer than waters at this same depth level in the SCS [*Quadfasel et al.*, 1990; *Gamo et al.*, 2007; *Tessler et al.*, 2010], and so results in unique geochemical properties with implications for carbon uptake within the deep Sulu Sea [*Chen et al.*, 2006]. The mean θ measured just ~10 m above the sill depth is 9.79°C in Mindoro Strait (at 450 m) and 9.81°C in Panay Strait (560 m) in excellent agreement with the hydrographic surveys. However, the benthic temperature shows substantial variability over the mooring deployment period (Figure 4). The range of 8.72°–10.94°C and standard deviation σ = 0.42°C of bottom θ at Mindoro Strait is much larger compared to Panay Strait with a range of 9.52–10.08°C and σ = 0.11°C, and Tablas Strait

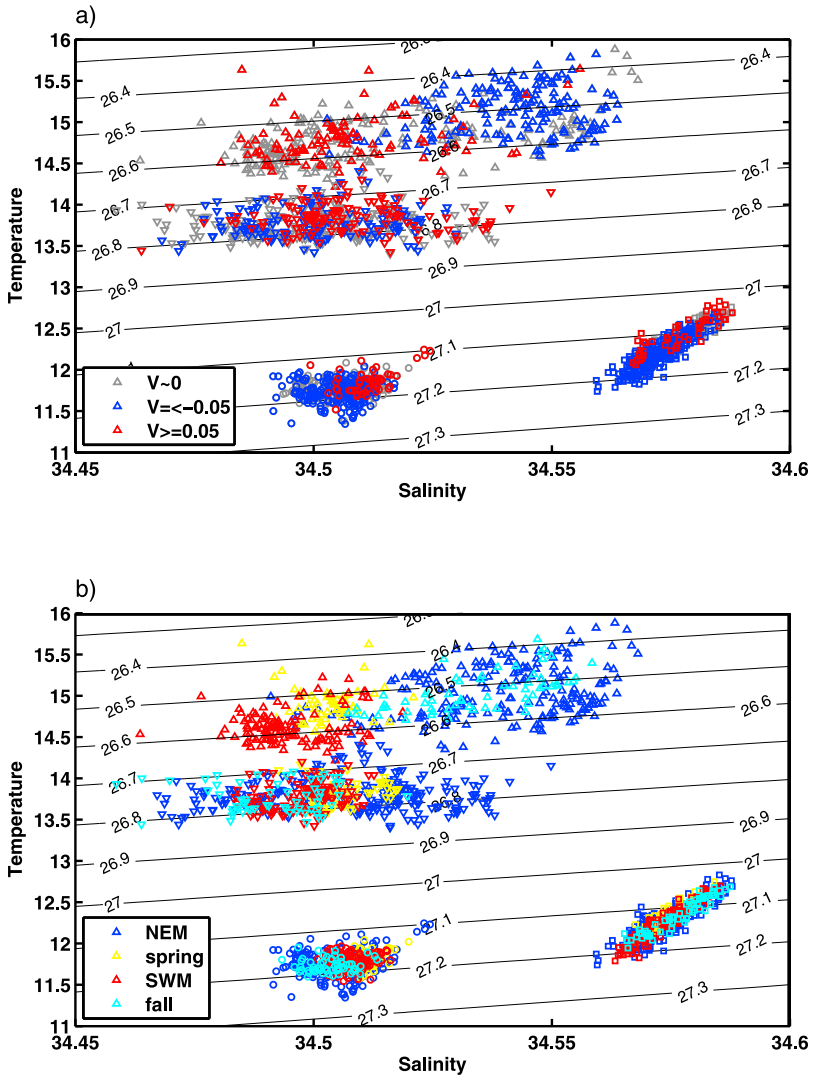

Figure 3. The temperature-salinity characteristics at 206 m (up triangle) and 312 m (squares) in Mindoro Strait, and at 244 m (down triangle) and 345 m (circles) in Tablas Strait color-coded by (a) velocity (V) and (b) season. In Figure 3a, V < −0.05 m s^{-1} is blue, V > 0.05 m s^{-1} is red, and V ∼ 0 m s^{-1} is gray. In Figure 3b, measurements during the Northeast monsoon (December–March) are blue, yellow during spring (April–May), red during the Southwest monsoon (June–September) and cyan during fall (October–November).

with a range of 10.05°–10.6°C and σ = 0.11°C. Thus, even though the sill depth at Mindoro is ∼100 m less than either Panay or Tablas sill depths, the bottom temperature at Mindoro is much cooler when there is stronger southward flow from the SCS. Conversely, during periods of weak or northward flow within Mindoro Strait, temperatures are warmer and similar to those found in Panay and Tablas. This tendency may reflect the higher levels of entrainment and mixing occurring downstream of the sills [*Quadfasel et al.*, 1990; *Tessler et al.*, 2010] that results in higher temperatures and salinities than found on corresponding depth layers within the SCS. Although we lack concurrent ASV information on the sill in Tablas Strait, *Gordon et al.* [2011] shows the deep Sibuyan Sea has a similar potential temperature of 10.4°C to the Tablas Strait mean of 10.3°C, suggesting that there could also be significant exchange between this sea and the deep waters observed in Tablas Strait.

4. Transport Variability

[18] Our primary goal is to provide a meaningful estimate of the mass flux through each of the instrumented straits that connect the Sulu Sea to the SCS and so provide the first observed time series of the magnitude and exchange of the transport. Unfortunately, single-point mooring measurements such as made during PhilEx, can compromise the integration of the depth and across-passage interpolation of the along-channel flow needed to compute accurate transport estimates (i.e. $\iint ASVdxdz$). The mooring point velocity observations need to be (1) laterally extrapolated across the passage to the strait sidewalls, and (2) vertically extrapolated where there may be gaps with depth. In this section, before

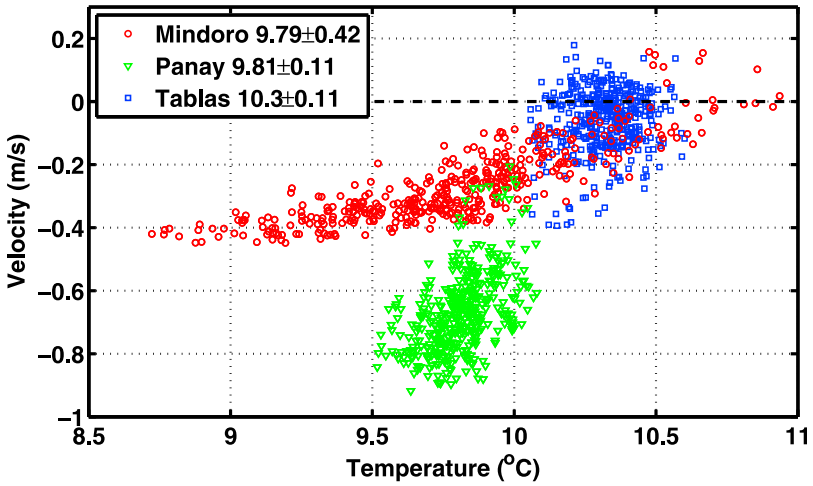

Figure 4. Near-bottom velocity versus near-bottom temperature in Mindoro Strait (red circle), Panay Strait (green triangle) and Tablas Strait (blue square). The temperature and velocity at Mindoro and Panay are measured at concurrent near-bottom depths of 450 m and 560 m respectively. In Tablas Strait, the temperature is measured near-bottom at 570 m and velocity at 360 m.

describing the transport variability with depth through each passage, we first discuss how we will handle the missing flows in the surface and bottom layers, as well as the cross-sectional velocity structure. Choices for the extrapolation schemes will be guided by the available shipboard ADCP and L-ADCP velocity sections made in each passage, the HF Radar data, and model output. Nonetheless, there are errors associated with each scheme and these will be discussed and detailed with respect to their impact on the transport estimate.

4.1. Assumptions for Transport Calculations

[19] Because of surface reflection contamination, upward-looking ADCPs are unable to resolve the very near surface velocity. During Philex, the ADCPs in Tablas Strait and Mindoro Strait that measured the upper layer flow were located at mid-water column depths (Figure 2), and hence only the velocity in the upper 20 m was missed. In these two straits, the surface gaps were filled assuming a constant velocity equal to the shallowest measured velocity (i.e., a "slab" extrapolation). The bottom-mounted configuration of the ADCP in Panay Strait (Figure 2) missed the upper 40 m of the near-surface layer. In Panay Strait, some information of the near surface circulation is available from the HF Radar measurements. The HF Radar data provides concurrent velocity measurements over the period 30 July 2008 to the recovery of the Panay mooring on 16 March 2009 (Figure 5a). The agreement between the surface ASV from the radar ($ASV_{z=0}$) and the resolved mooring measurement at 50 m ($ASV_{z=50}$) is quite good (r = 0.62). A least squares fit of the data gives $ASV_{z=0} = 0.06 + 0.63ASV_{z=50}$. This least squares fit will be used to fill in the missing surface values in Panay Strait, and we then assume a linear fit for the missing mooring ASV at depths between the surface and 50 m.

[20] The missing velocity at the ocean bottom also needs to be accounted for in the transport calculations. In Mindoro and Panay Straits, only the bottom 20 m is missing. Two extrapolation schemes were considered. Given the strong benthic flows observed on the sills at these mooring sites, the first scheme assumed a slab model and assigned the deepest measured velocity to the missing data below, assuming zero velocity at the bottom. A second scheme applied a constant shear from the deepest measured velocity to zero velocity at the bottom. Bottom measurements from discrete L-ADCP casts in the direct vicinity of the sill at Mindoro (Figure 6a) and Panay (Figure 6b) Straits show casts where both schemes might be representative of the true bottom flow. In Tablas Strait, because of the failure of the near-bottom ADCP (Figure 2), filling the missing lower 200 m of the water column is more problematic. A one-time shipboard ADCP survey just north of the sill in Tablas Strait during December 2007 (Figures 7k–7l) suggests a relatively quiescent benthic flow in this passage. Similarly, the 1/12° global HYCOM model shows relatively weak (<0.05 m s^{-1}) flow in the lower layer directed toward the Sulu Sea in the annual mean [*Hurlburt et al.*, 2011]. Both a slab layer and a constant shear model were used to extrapolate the missing bottom velocities for the transport calculations in Tablas Strait. Errors in the transport estimates of the lower layer in Tablas Strait can also be assessed in light of any differences between the deep Mindoro and Panay transports: given the geometry of the straits (Figure 1b), it is reasonable to assume to first order through conservation requirements, that any bottom flow through Panay Strait not supplied by Mindoro Strait possibly should have been supplied by Tablas Strait. Of course, residency time or storage within the Semirara Sea is not accounted for in this simple scenario.

[21] Perhaps the largest contributor to the errors in the transport calculations is the extrapolation of the ASV measured at the single mooring site in each passage to the strait sidewalls. The cross-passage shipboard transect velocity measurements offer some guidance for the extrapolations (Figure 7). In each case, the ADCP transects were generally conducted between each of the channel sidewalls and orthogonal to the along-channel flow. However, whereas the moored velocity measurements are continuous over ~15–18 months, the ADCP transects are mostly discrete

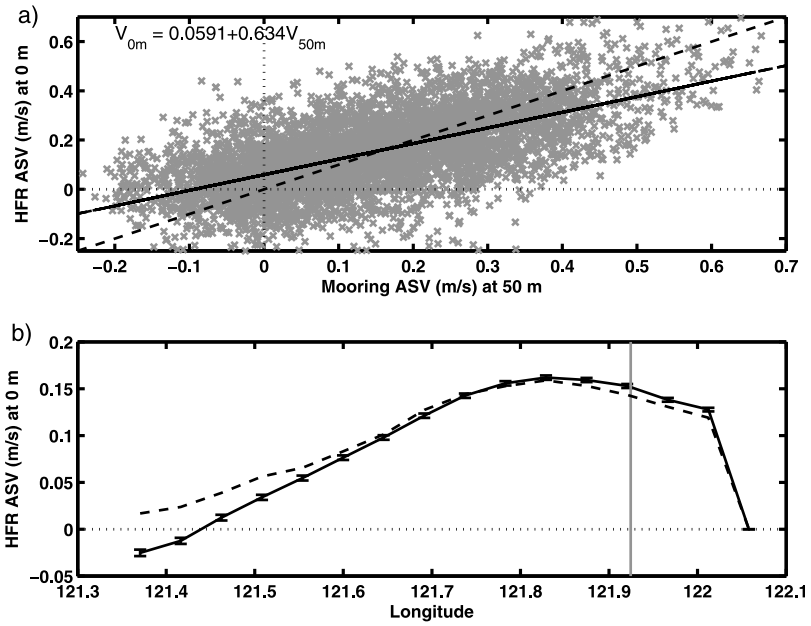

Figure 5. (a) Scatterplot of the ASV measured at 50 m depth on the Panay Strait mooring and at the surface by the HF radar at the Panay mooring location. Black dashed line shows the 1:1 curve, and heavy black line shows the least squares fit of the mooring velocity at 50 m depth to the HF Radar velocity at the surface. (b) The average (black), standard error (black bars) and median (dashed) ASV measured by the HF radar across a transect along 11.26°N. The Panay Strait mooring is located along this transect at 121.92°E (gray line).

short period surveys albeit over different phases of the tidal and monsoon cycle. In Mindoro (Figures 7a–7d) and Panay (Figures 7e–7h) the shipboard surveys were 24-h repeat transects and so the averaging removes some of the higher frequency tidal signals. In Tablas Strait (Figures 7i–7l) however, only single one-time ADCP transects are available. Changes in the cross-channel flow structure can occur over relatively short time periods, although in general changes in the vertical structure of the ADCP velocity agreed well with the concurrent subinertial ASV profile measured at the mooring site over the same time period (Figure 7). Thus with these caveats in mind, in the following we use the ADCP velocity transects that to date provide our best and only option to explore the observed cross-sectional, along-strait flow within each of the narrow channels needed for the transport integration.

[22] All the available ADCP and L-ADCP surveys denote ASV variability occurs over different depth ranges at different times across each passage on either side of a mooring site (Figures 6 and 7). In Mindoro Strait, the L-ADCP casts

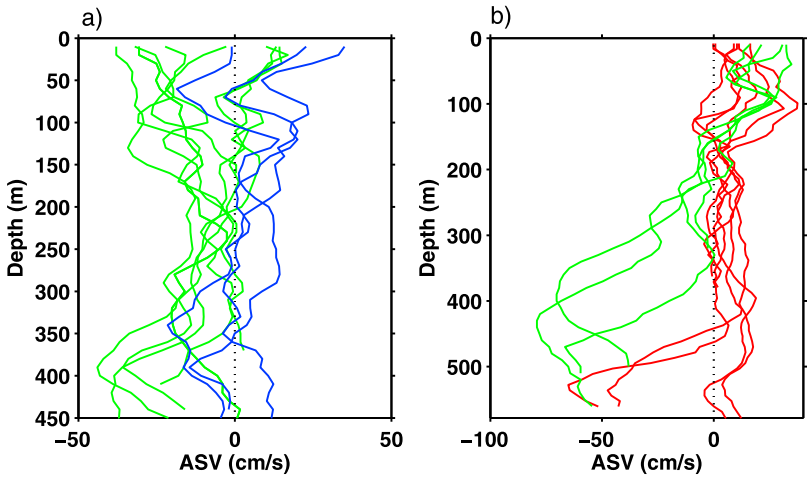

Figure 6. ASV (cm s^{-1}) measured by the L-ADCP in the vicinity of the sill in (a) Mindoro and (b) Panay Straits during June 2007 (red); January 2008 (green); and March 2009 (blue). Note the different depth axes.

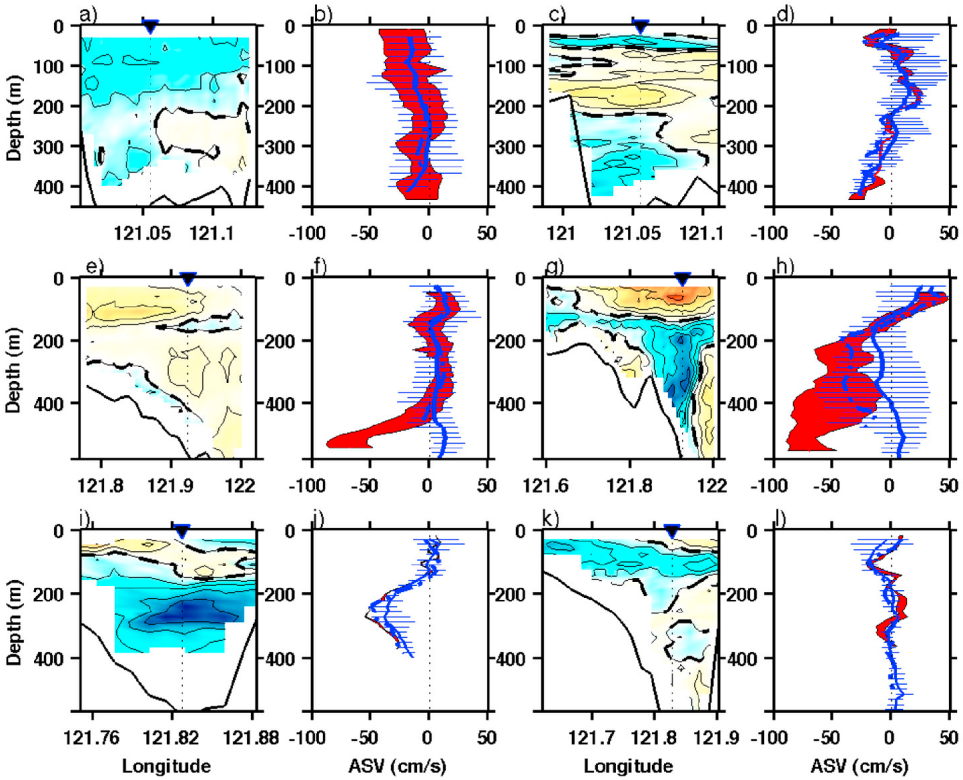

Figure 7. ASV (cm s^{-1}) from shipboard ADCP surveys in (a–d) Mindoro, (e–h) Panay, and (i–l) Tablas Straits. The first and third columns show the velocity section across the strait (zero contour is heavy dashed, and contour interval is 10 cm s^{-1}) with the mooring location indicated by the diamond on the top axis. The second and fourth columns show the average (blue solid) and standard deviation (blue horizontal bars) ADCP ASV profile across the strait; the ADCP ASV profile nearest the mooring (blue dashed); and the range of ASV measured by the mooring over the time of the ADCP survey (red). The ADCP surveys were conducted in February 2008 (Figure 7a); March 2009 (Figure 7c); June 2007 (Figure 7e); February 2009 (Figure 7g); February 2008 (Figure 7i) and December 2007 (Figure 7k).

(Figure 6a) and repeat shipboard ADCP surveys (Figures 7a and 7c) show a surface to intermediate depth layer that varies in cross-passage structure from cruise to cruise, although the mean cross-passage ASV profiles (thick blue lines in Figures 7b and 7d) fall within the range of ASV measured at the mooring site during the time of the ADCP surveys (red zone in Figures 7b and 7d). This suggests that, at least at the time of the surveys, the occasional opposing flows on either side of the mooring largely cancel out when considering the flow structure across the channel. In the benthic layer of Mindoro Strait, both the ADCP casts (Figures 7a and 7c) and model results [*Hurlburt et al.*, 2011] suggest enhanced southward flow probably occurs just west of the mooring location. This westward intensification is likely a result of the channel geometry that is northwestward upstream of the mooring site toward the deep inflow from the SCS (Figure 1b). Recall also that the mean deep ASV measured at Mindoro (Figure 2a) was substantially less than that measured at Panay (Figure 2b). Hence the benthic transport estimated from the ASV at the Mindoro mooring site will probably underestimate the total deep transport contribution through this passage. In Panay Strait, the June 2007 ADCP survey (Figure 7e) suggests enhanced upper layer flow occurs west of the mooring, and the yearlong average surface ASV measured by the HF radar across a zonal section at 11.26°N also shows slightly stronger flow occurs to the west of the mooring site (Figure 5b). However, the western intensification is not present during the February 2009 (Figure 7g) ADCP survey, and as in Mindoro Strait, the mean ADCP ASV profiles are mostly within the range of ASV measured contemporaneously at the mooring site, particularly those ADCP profiles in nearer proximity to the mooring (Figures 7f and 7h). This suggests that the mooring in Panay Strait was favorably located to capture the deep overflow into the Sulu Sea. The two one-time shipboard ADCP surveys in Tablas Strait also show the vertical structure of the cross-channel averaged ADCP measurements has fairly good agreement with the concurrent ASV measurements at the Tablas mooring site (Figures 7i–7l).

[23] The shipboard ADCP and L-ADCP surveys suggest three possible schemes for the cross-passage extrapolation (in 1-km bins) of the mooring ASV data in each passage: (1) linear interpolation from the mooring across the passage (denoted linear in the following); (2) assign the measured ASV to the half-width of each passage, centered about the mooring location (half-width); and (3) extrapolate uniformly across the whole passage (full-width). In all transport schemes, zero flow is assumed in the last kilometer bin nearest the sidewalls, suggesting an effective channel width that is slightly less than the topographic width (see Table 1).

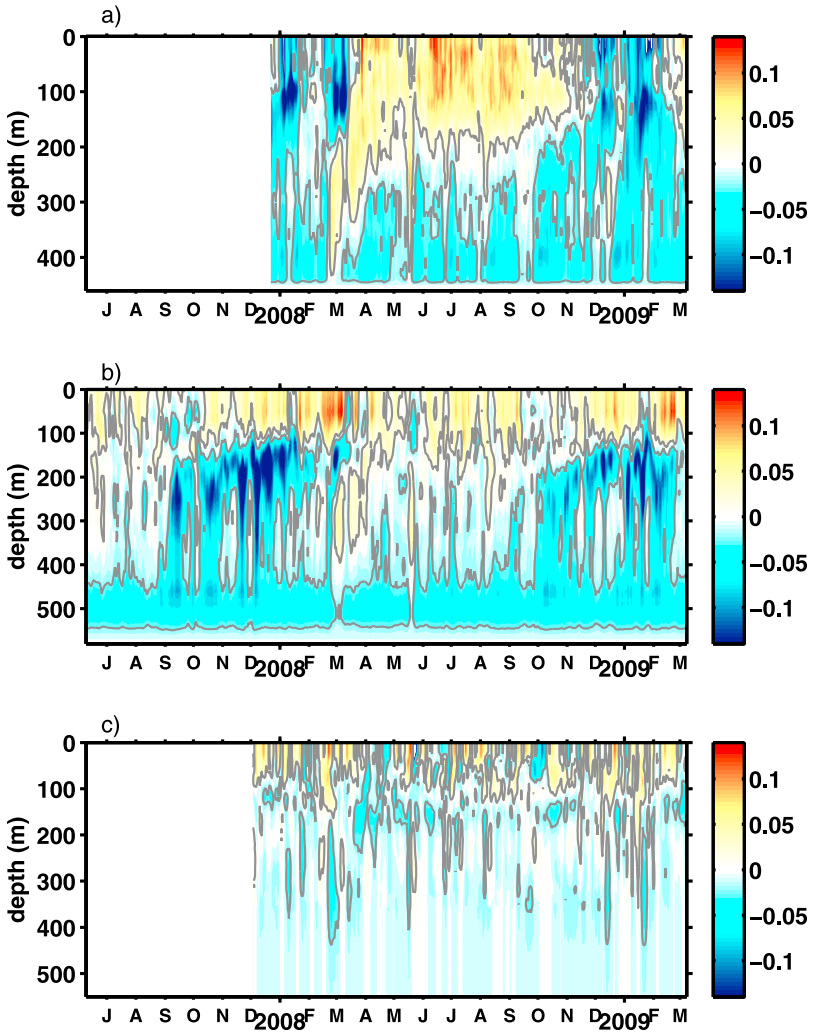

Figure 8. Vertical distribution of transport per unit depth (Sv m^{-1}) for (a) Mindoro, (b) Panay, and (c) Tablas Straits to their respective sill depths. Gray contours are shown at +/−0.02 Sv m^{-1} (solid/dashed lines).

This conforms to the shipboard ADCP measurements in each passage (Figure 7) and the HF radar surface measurements in Panay Strait (Figure 5b) that show little sidewall boundary effects. Here we use the *Becker et al.* [2009] 30-arc second bathymetry to determine the strait area between the 100 m isobaths on either side of each channel for the transport calculations, thus neglecting the shallow shelf regions to the west of Panay and Tablas Straits and either side of the Mindoro mooring site (Figure 1b).

[24] In the following, we show transports calculated using the surface extrapolations in each strait noted above, a slab layer for the missing bottom layers, and the full-width extrapolation across the passage. These schemes are considered to give our best transport estimates. As noted, the errors are likely to be largest for our cross-passage extrapolations, particularly in the surface layer transports where the passage is widest. Collectively the lateral schemes provide a range of possible transport values: the half-width scheme will likely be a mid-range estimate between the possible lower bound from the linear extrapolation and the upper bound from the full-width extrapolation. The range of transports using each scheme will be reported as our uncertainty error. In addition, we will also address the impact on the transport estimates of the missing bottom measurements in Tablas Strait and the sub-optimal location of the Mindoro mooring site slightly east of the likely benthic ASV maximum, and the implications of these for the observed deep overflow captured in Panay Strait.

4.2. Vertical Distribution of Transport

[25] The upper layer transport in Mindoro Strait is dominated by an annual cycle, with strong northward transport from the surface to ~170 m during the SWM of boreal summer, and strong southward transport appearing in two distinct pulses each of about 3 weeks duration during the two surveyed NEMs (Figure 8a). In contrast, the upper layer transport in Panay Strait has a more episodic nature throughout the entire deployment period (Figure 8b), although in general the transport is northward, stronger during the late NEM and with weak southward transport evident during the fall transition (September–October). Similarly, in Tablas Strait the upper transport time series

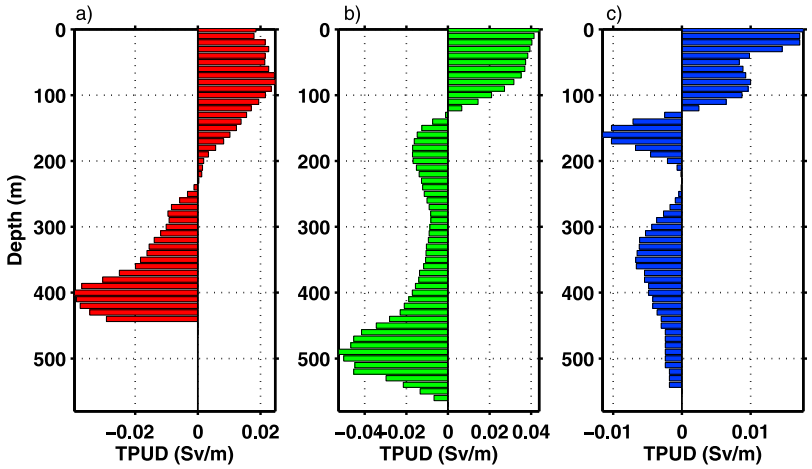

Figure 9. Transport per unit depth (Sv/m) in 10-m intervals for (a) Mindoro, (b) Panay, and (c) Tablas Straits. All panels are plotted to the bottom depth of Panay Strait. Note different scales on *x* axis.

shows no clear monsoonal relationship, and is characterized more by short-period variability on time scales of 10–20 days (Figure 8c).

[26] The most striking feature of the Panay transport time series is the intermediate depth core of strong flow toward the Sulu Sea that begins during the fall transition (September–October) and lasts through to the end of the NEM (Figure 8b). Similar strong subsurface pulses occur in Mindoro Strait during the NEM that are separated from the upper layer southward pulses by a region of weaker transport (Figure 8a). Since the subsurface cores occur during both of the surveyed NEMs in Panay and Mindoro Straits, this suggests a monsoonal relationship, rather than an isolated event phenomenon. Initially during the fall transition, the top of the subsurface core in Panay Strait is found at ~180 m depth and progressively shoals to ~100 m depth by the end of the NEM. A similar shoaling is apparent in Mindoro Strait during the survey period, although the transport during the fall transition is not as strong and the strongest NEM cores are slightly higher up in the water column compared to those in Panay Strait. In Tablas Strait the intermediate depth transport is mostly toward the Sulu Sea nearly year-round, with a hint of deeper reaching southward transport during the NEM (Figure 8c) corresponding to when the stronger intermediate depth southward transport occurs in Mindoro and Panay Strait (Figures 8a and 8b).

[27] Although the strongest southward transport is associated with the intermediate depth cores in Mindoro and Panay Straits, below this the transport is largely toward the Sulu Sea (Figures 8a and 8b). The bottom intensification of the transport in both straits is associated with the benthic overflows that act to ventilate the Sulu Sea to ~1250 m depth [*Tessler et al.*, 2010]. In Mindoro Strait, the benthic overflow results in a slight secondary transport maximum near bottom (Figure 8a). Whereas downstream in the deeper Panay Strait, the deep secondary transport maximum appears stronger at ~520 m (Figure 8b), consistent with the mean ASV observations that show the southward ASV maximum occurs ~50 m above the sill (Figure 2b).

[28] Isolated intermediate depth northward reversals in transport are evident in both Mindoro and Panay Straits during late February–early March 2008 and again in mid-May 2008 (Figures 8a and 8b). When these intermediate depth reversals occur, the southward transport in the benthic layer of each strait is considerably reduced. Weaker intermediate depth northward reversals are also observed in Tablas Strait during these same time periods (Figure 8c). Clearly in Mindoro and Panay Straits, the northward flow appears first at depth, and this is then followed by northward flow at shallower depths. This upward phase propagation is a characteristic signature of downwelling Kelvin waves [e.g., *Sprintall et al.*, 2009]. The possible impact of these large-scale planetary waves on the transport variability within the Philippine archipelago will be discussed further in section 5.

[29] The mean transports in each 10-m depth layer (Figure 9) will help guide our choice of depth layers for examining the integrated transport time series and their relationship between the three straits. Ideally we would like to examine the vertical distribution of the transport in terms of density layers, as this classification would more clearly indicate the most plausible pathways for the circulation and more readily provide evidence of any vertical redistribution of the fluxes through mixing. Unfortunately full-depth temperature and salinity profiles were not possible on the moorings in these narrow and dynamic passages. Nonetheless, the profiles of the mean transport with depth in each passage provide an informative first look at the vertical partitioning of transport between the three Philippine straits. Both Panay (Figure 9b) and Tablas Straits (Figure 9c) show a similar mean vertical structure with three-cores, albeit of different magnitude. Northward transport occurs in the upper layer down to 130 m, with an intermediate depth core of southward transport and below that, a second core of southward transport that in Panay Strait is associated with the sill overflow. In contrast, the vertical structure in Mindoro Strait shows a distinct two-layer structure with northward transport in the upper 230 m and southward transport below (Figure 9a). As in Panay Strait, the strongest core in Mindoro Strait is associated with the sill overflow. Simple conservation arguments would suggest that the northward transport in the upper layer from the Sulu Sea through Panay Strait exits via both Tablas and Mindoro Straits. Similarly, it might be argued that the intermediate depth core of southward transport from Tablas Strait

Table 2. Monthly Averaged and 2008 Total Transports (Sv) Over Depth Ranges 0–130 m, 130–250 m, 250 to Bottom and Full Depth in Mindoro, Panay and Tablas Straits

Mooring	Jan	Feb	Mar	Apr	May	Jun	Jul	Aug	Sep	Oct	Nov	Dec	Total
						Transport (0–130 m)							
Mindoro	−0.94	−0.47	−0.23	0.84	0.56	1.17	1.00	1.04	0.77	0.45	0.06	−0.76	0.29
Panay	0.31	0.79	0.30	0.50	0.08	0.45	0.61	0.48	0.29	0.17	0.35	0.65	0.41
Tablas	0.13	0.32	0.20	−0.21	0.05	0.01	0.23	0.20	0.12	0.14	0.10	0.37	0.14
						Transport (130–250 m)							
Mindoro	−0.35	−0.10	0.41	0.36	0.19	0.28	0.22	0.33	0.15	−0.19	−0.31	−0.35	0.05
Panay	−0.75	−0.27	0.07	0.14	0.02	0.11	0.06	0.17	−0.01	−0.33	−0.60	−0.62	−0.17
Tablas	−0.07	−0.01	−0.13	−0.14	−0.09	−0.07	−0.03	−0.05	0.01	−0.10	0.05	−0.02	−0.05
						Transport (>250 m)							
Mindoro:	−0.56	−0.11	0.05	−0.56	−0.28	−0.50	−0.41	−0.55	−0.34	−0.85	−0.47	−0.36	−0.41
Panay	−0.81	−0.52	−0.03	−0.67	−0.38	−0.65	−0.69	−0.66	−0.76	−1.51	−0.94	−0.64	−0.69
Tablas	−0.18	−0.20	−0.14	−0.02	−0.02	−0.03	−0.09	−0.07	−0.15	−0.04	−0.21	−0.18	−0.11
						Transport (Full Depth)							
Mindoro	−1.85	−0.67	0.23	0.65	0.48	0.96	0.82	0.83	0.59	−0.58	−0.72	−1.45	−0.07
Panay	−1.25	0.00	0.34	−0.03	−0.29	−0.09	−0.03	0.00	−0.48	−1.67	−1.19	−0.61	−0.44
Tablas	−0.11	0.11	−0.07	−0.37	−0.06	−0.09	0.11	0.08	−0.01	0.00	−0.05	0.17	−0.03

(130–250 m) contributes to both the southward maximum in Panay Strait and also to the northward transport through Mindoro Strait over a similar depth range. Below 250 m the transport in each strait is southward, albeit with maximums at different depths (Figure 9). Clearly however, the benthic cores of southward flow in Mindoro and Tablas Straits must sink in the deep Semirara Sea before contributing to the benthic spill-over into the Sulu Sea via the deeper Panay Strait.

4.3. Transport Time Series Mean and Variability

[30] In this section we discuss the variability observed in the total transport time series for each passage over the three distinct layers evident in the mean transport of profiles of each passage (Figure 9 and Table 2): an upper layer (0–130 m); an intermediate depth layer (130–250 m) and the benthic layer (250 m – bottom). So as not to seasonally bias the reported annual means, the transports are all reported just for the calendar year 2008, a common and complete deployment period for all moorings (Table 1). The time series of layer and full-depth transports during 2008 is presented in Figure 10, while Table 2 reports the monthly averaged and total transports.

[31] In the upper 130 m, the strongest transports occur in Mindoro Strait. Relatively steady northward transport is found during the SWM and both monsoon transitions, while southward transport during the NEM tends to occur in ∼20 day-long bursts interspersed with periods of near-zero transport (Figure 10a). Transports during these NEM burst periods can reach 1–2 Sv. In Panay Strait the upper layer transport is primarily northward year-round (Figure 10a and Table 2). In 2008, the mean total upper layer transport through Panay Strait was 0.41 Sv away from the Sulu Sea, with approximately two-thirds flowing northward through Mindoro Strait (0.29 Sv) and one-third through Tablas Strait (0.14 Sv).

[32] At intermediate depths (130–250 m), the total transport through both Panay and Mindoro is highly correlated (r = 0.9, Mindoro leads Panay by 1 day) with relatively strong southward transport into the Sulu Sea beginning in the fall transition (∼October) and continuing through the NEM, and mostly northward transport during the spring and SWM (Figure 10b). However, the northward transport is stronger in Mindoro compared to Panay while the reverse is true of the southward transport. As a result the total transport at this intermediate depth range is 0.05 Sv northward in Mindoro and 0.17 Sv southward in Panay. Part of the deficit in the Panay southward transport during the SWM is probably provided by the excess southward transport in the upper layer through Mindoro Strait (Figure 10a). Recall that the core of the subsurface southward transport during this season is located higher in the water column in Mindoro compared to Panay (Figures 8a and 8b). In Tablas Strait the intermediate depth transport is dominated by intraseasonal variability, with a weak net southward transport of 0.05 Sv. This southward transport in Tablas Strait primarily occurs during the SWM (Table 2) and, along with the northward transport through Panay Strait (Figure 8b), probably contributes to the net northward transport through Mindoro during this season.

[33] In the benthic layer (250 m to bottom), the transport time series through Panay and Mindoro Straits again largely track each other (Figure 10c), and reflect the strong bottom overflows into the Sulu Sea. The benthic transport is slightly stronger southward in both straits during the fall transition (Table 2). Interestingly there is a significant correlation (r = −0.7) between Mindoro and Tablas Strait, with Mindoro lagging Tablas by 1 day. The negative correlation suggests that when transport is southward through Mindoro it is northward through Tablas, and vice versa. Recall this deeper layer below 360 m was not directly sampled in Tablas Strait, although the transport estimates for the assumption of a bottom slab layer suggest only weak and variable transport. In addition, there is mostly good agreement between the extrapolated transport estimate for Tablas Strait (solid blue line in Figure 10c) and the estimate required to balance the bottom transport through Mindoro Strait with the overflow at Panay Strait (dashed blue line in Figure 10c). Only during the fall transition when the Panay spill-over is strongest and during the event in late-February is there a considerable

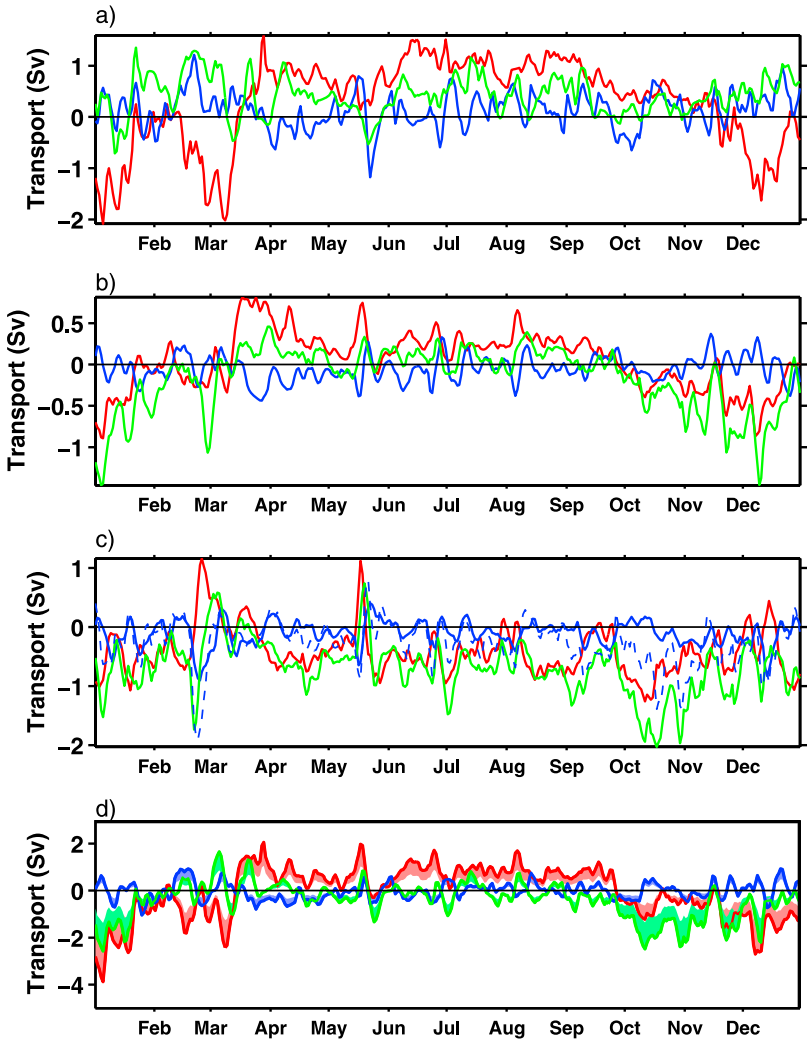

Figure 10. Time series of transport (Sv) for Mindoro Strait (red), Tablas Strait (blue) and Panay Strait (green) for the depth interval (a) 0–130 m, (b) 130–250 m, (c) 250-bottom, and (d) full depth. Note the change in transport scales in each panel. The Panay minus Mindoro transport over the 250-bottom depth range is the dashed blue line in Figure 10c.

discrepancy between the Panay-Mindoro residual and the extrapolated transport for Tablas Strait. The total 2008 mean benthic-layer transport is southward through all straits: −0.41 Sv in Mindoro, −0.11 Sv in Tablas and −0.69 Sv in Panay Strait (Table 2). As noted, the excess southward transport through Panay Strait (0.17 Sv) may be because of the missing deep contribution through Tablas Strait particularly during the fall transition, and/or the underestimate through Mindoro Strait because the mooring was likely located east of the main benthic core (viz. Figures 7a–7d).

[34] The full-depth transports show that both Panay and Tablas are near zero during the SWM when Mindoro is primarily northward (Figure 10d). During the fall transition and NEM the strong intermediate depth pulses enhance the southward benthic transport and dominate the total transports in Panay and Mindoro. Although significant total transport events over 2 Sv can occur both northward and southward, the mean total transports are very small and southward toward the Sulu Sea. During 2008 the mean and standard deviation of the total transport time series were −0.07 (±1.11) Sv in Mindoro Strait, −0.03 (±0.36) Sv in Tablas Strait and −0.44 (±0.77) Sv in Panay Strait.

[35] Our discussion of the total transports through the Philippine Straits is based on calculations assuming a slab layer for the missing bottom layers and extrapolation of the mooring data across the full-width of the passage. The total transport for the extrapolations that include a constant shear for the bottom layer, and the half-width and linear cross-passage schemes is shown in Table 3, while the minimum and maximums for the total daily transport time series using the different schemes is shown by the shading in Figure 10d. In Panay and Mindoro Straits there is little difference in the total transports dependent on the choice of fill for the bottom layers (Table 3) because only the lower 20 m was missing direct velocity measurements in these channels. In contrast, in Tablas Strait the missing lower 200 m of the water column results in an order of magnitude difference in total transport for the full-width cross-passage scheme dependent on the use of a slab or shear extrapolation (Table 3). In Mindoro Strait the total transport of −0.07 Sv using the full-width

Table 3. Transport Estimates for the Slab and Constant Shear Bottom Layer, and the Full-Width, Half-Width and Linear Schemes for the Cross-Passage Extrapolation in Mindoro, Panay and Tablas Straits

Transport Scheme	Mindoro Strait Transport (Sv)	Tablas Strait Transport (Sv)	Panay Strait Transport (Sv)
Full-width, slab bottom	−0.07	−0.03	−0.44
Full-width, shear bottom	−0.06	−0.00	−0.44
Half-width, slab bottom	−0.11	−0.03	−0.38
Half-width, shear bottom	−0.10	−0.02	−0.38
Linear width, slab bottom	−0.04	−0.01	−0.26
Linear width, shear bottom	−0.03	−0.01	−0.26

scheme lies midway between the estimates using the cross-passage linear (−0.04 Sv) and half-width (−0.11 Sv) extrapolation schemes (Table 3). This is simply a result of the channel geometry: while both the half-width and full-width schemes capture the strong bottom flows in this passage, the full-width scheme also results in more northward transport in the wider upper layer, and this reduces the total full-width transport estimate compared to the half-width scheme. Conversely, in Panay Strait, the full-width total southward transport (−0.44 Sv) is stronger than either the linear (−0.26 Sv) or the half-width (−0.38 Sv) transport estimates (Table 3). As in Mindoro Strait this is because of the channel geometry afforded by the full-width extrapolation, although in the case of Panay Strait the stronger southward transport is because of the increased contribution at intermediate depths during the NEM (Figure 10b).

5. Discussion

[36] Moorings deployed during the PhilEx field program provide the first time series of observed velocity and properties in the major straits that connect the SCS to the Sulu Sea. The rich and varied time series reveal a complex response to both the surface monsoonal forcing and the bathymetrically controlled deep bottom overflows. Here we discuss the possible dynamics responsible for the observed transports within the three straits.

5.1. Upper Layer

[37] The upper layer circulation within the confluence region of the three passages appears to be very complex. In Mindoro Strait, the seasonal signal is readily apparent with relatively steady northward flow persisting during all of the SWM, while the shorter NEM is characterized by strong southward pulses that last for ∼20 days and are interspersed by periods of weak or slight flow reversal. However, the flow direction is opposite to that expected as due to an Ekman response to the prevailing monsoon winds. This suggests that the upper layer flow in Mindoro Strait may largely be in response to remote wind-forcing and/or that the Ekman layer is thin and so not well resolved by the ADCP velocity measurements in the very near-surface layer. In a series of ROMS modeling experiments, *Han et al.* [2008] found both these reasons to be the case, and suggested that ∼65% of the upper layer transport variance in Mindoro Strait is attributable to remote forcing from both the Pacific Ocean and the SCS, but mostly the latter. Both models [*Lebedev and Yaremchuk*, 2000; *Yaremchuk et al.*, 2009; *etc*] and surface drifter data [*Centurioni et al.*, 2004; *Fang et al.*, 2005] show surface flow is strongest into the SCS in NEM as a result of a pressure head across Luzon Strait [*Metzger and Hurlburt*, 1996]. However, relatively few surface drifter trajectories show a direct route from Luzon Strait southward along the west coast of Luzon Island [*Centurioni et al.*, 2004; *Fang et al.*, 2005; *Ohlmann*, 2011], and no drifter trajectories passed through Mindoro Strait (although this may also be due to unplanned recoveries by fishermen etc.). The positive wind stress curl in NEM results in a basin-wide cyclonic gyre [*Shaw and Chao*, 1994; *Ho et al.*, 2000; *Fang et al.*, 2005] that is also clearly evident in the sea surface height anomalies (SSHa) during 2008 (Figure 11). The southward transport through the upper layer in Mindoro Strait during the NEM therefore could be derived from the southern limb of this gyre.

[38] The reason for persistent northward upper-layer flow in Mindoro Strait during the SWM remains unclear, however most models also report northward or reduced transport during this season [e.g., *Fang et al.*, 2005; *Han et al.*, 2008; *Yaremchuk et al.*, 2009; *Hurlburt et al.*, 2011; *Liu et al.*, 2011]. A similar pattern is found for the seasonal upper layer flow through Mindoro Strait in the average 2004–2009 1/12° global HYCOM-18.2 results [*Hurlburt et al.*, 2011]. *Han et al.* [2008] show the northward flow through Mindoro Strait in SWM is fed by a northward jet along the west coast of Panay, as supported by the surface current climatology of *Wyrtki* [1961]. However, while the mean surface transport in Panay Strait is northward, it does not show the persistent northward flow during the summer monsoon evident in Mindoro Strait (Figure 10a), suggesting this jet is not a permanent feature during this period. Nonetheless, it is likely that at times the northward surface transport through Mindoro in the SWM is fed by both northward flow from Panay Strait, and perhaps also by southward surface flow through Tablas Strait that is stronger during the early part of this monsoon phase (Figure 8c and Table 2).

[39] Regional wind-forcing may play an additional role in the upper layer transport variability within each strait. Mountain gaps along the Philippine archipelago result in alternating bands of positive and negative wind stress curl from north to south within the eastern SCS and Sulu Sea during the NEM (Figures 11a, 11b, and 11f) that respectively spin-up pairs of cyclonic and anticyclonic eddies [*Pullen et al.*, 2008; *Wang et al.*, 2008; *May et al.*, 2011]. Upper layer transport (0–130 m) in Mindoro Strait is significantly correlated ($r = -0.7$) with the wind stress curl of the region in the southeast SCS just west of Mindoro Island: the positive wind stress curl pattern and the resulting cross-strait sea level gradient (Figures 11a, 11b, and 11f) results in southward flow through Mindoro Strait. Furthermore, *Pullen et al.* [2011] found that wind stress surges characterized by a more easterly component are associated with stronger

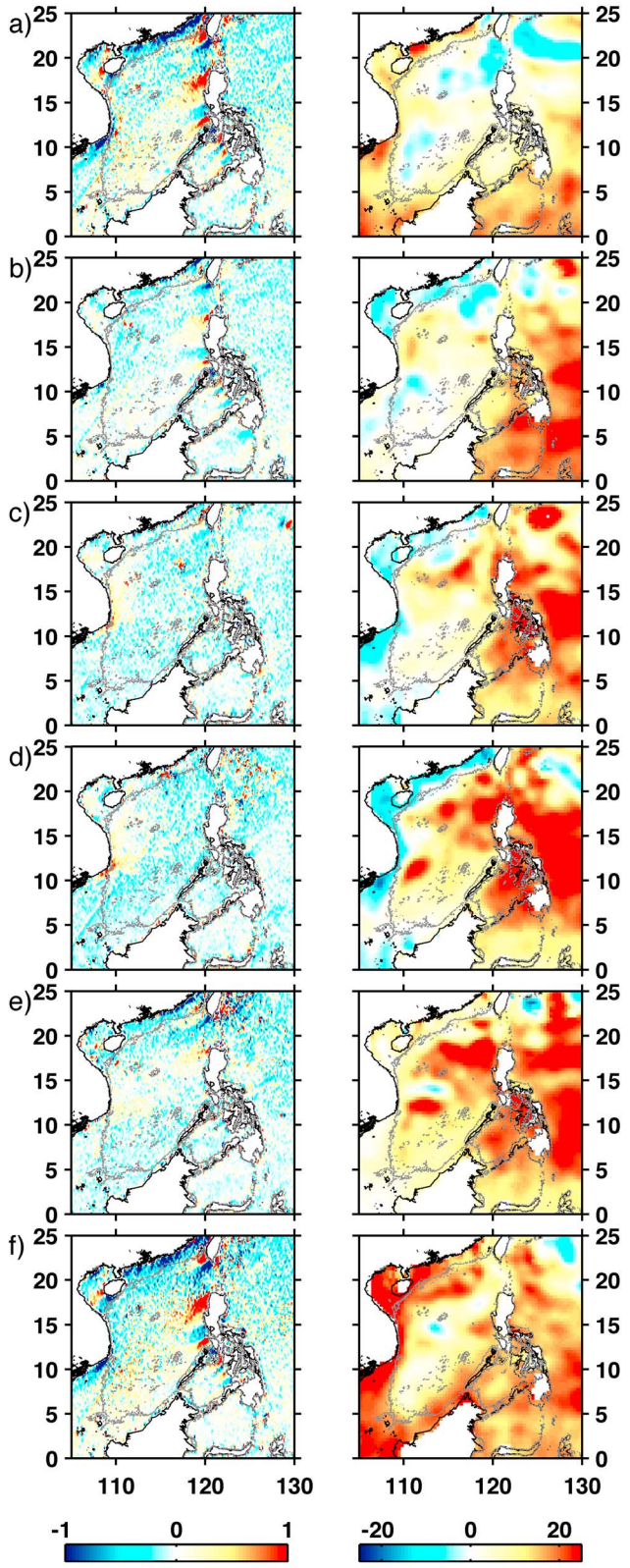

Figure 11. Wind stress curl (10^6 N m^{-3}) and sea surface height anomaly (cm) during 2008, averaged over (a) January–February, (b) March–April, (c) May–June, (d) July–August, (e) September–October, and (f) November–December. The 100 m isobath is indicated by the gray line.

southward flow through Mindoro Strait, while surges with a more northerly component disrupt the geostrophic balance and lead to more northward flow through the strait. The wind surges are typically separated by 12–17 days [*Pullen et al.*, 2008, 2011] consistent with the duration of the transport pulses observed in the upper layer through Mindoro Strait during the NEM (Figure 9a). Similarly, local winds can shift the location of the jets and eddies also prevalent in the northeastern Sulu Sea [*Pullen et al.*, 2008; *Han et al.*, 2008; *Gordon et al.*, 2011], and subsequently lead to the intermittent reversals and more variable upper layer transport observed in both Panay and Tablas passages.

5.2. Intermediate Depths

[40] Perhaps the most outstanding feature of the transport time series is the strong southward flows observed at intermediate depth in Mindoro and Panay Straits (Figures 8a and 8b). Both Mindoro and Panay show the strong southward pulses at ~200–300 m depth beginning in October 2008 with opposing (Mindoro) or weak (Panay) flow found in the upper layer. As the NEM reaches its peak, these subsurface pulses gradually strengthen and shoal to occur near the bottom of the thermocline at 100–200 m depth in Mindoro Strait (Figure 8a) and 130–230 m in Panay Strait (Figure 8b). The shallower cores at Mindoro Strait may possibly be a result of the mooring being located east of the main flow through this passage. Occasionally the pulses are connected to the strong southward flows found in the benthic layer of both straits (e.g., January 2009). Since these pulses occur during both of the fall to NEM sampled during the 2007–2009 mooring deployment period it appears likely that they are related to the large-scale monsoonal forcing. While southward flow occurs over similar depth ranges in Tablas Strait (Figure 8c), the flow is considerably weaker and can occur during any month of the year, and hence the Sibuyan Sea is unlikely to be a source of this variability. Furthermore, the intermediate depth range rules out a direct Pacific source as it is well below the shallow sill depth of San Bernardino Strait. Indeed, the T-S properties in Mindoro Strait show this southward flow during fall and NEM is associated with inflow of the saltier and warmer Subtropical Lower Water mass from the SCS (Figure 3). Thus, it appears most likely that the SCS is the source of the southward pulses during the fall and NEM.

[41] The time series of intermediate depth (130–250 m) transport in Panay Strait (Figure 8b) shows significant correlation with SSHa within the SCS (Figure 12). Similar correlation patterns are found for the 0–130 m and 130–250 m transport time series in Mindoro Strait (not shown). The correlation patterns are of the sense that negative correlations correspond to high SSHa and southward transport through the strait. The fall transition from the SWM to the NEM marks the strongest change in the annual wind stress cycle in the SCS [*Shaw and Chao*, 1994]. The wind reversal develops first in the northern SCS in September, raising the local sea level and setting up an alongshore pressure gradient forcing the southwestward propagation of coastally trapped waves along the western boundary of the SCS [*Shaw and Chao*, 1994; *Qu*, 2000]. Off the coast of Vietnam, the southwest current meets a surface-intensified northward coastal jet that is present here during the SWM and prevents further southward flow, but rather the current

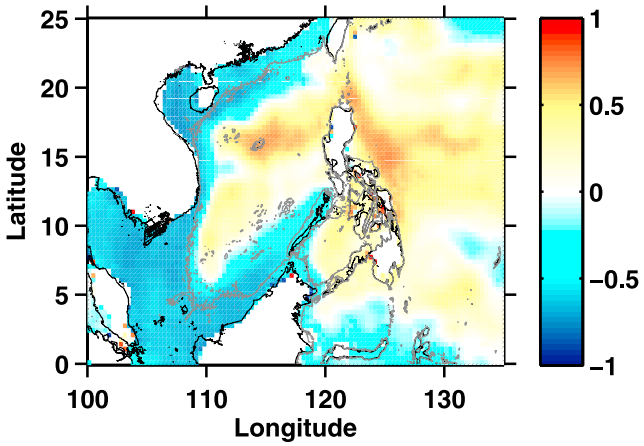

Figure 12. Correlation map of transport at 130–250 m depth in Panay Strait with regional sea surface height anomaly. Correlations that are not significant at the 95% confidence limit are white. The 100 m isobath is indicated by the gray line.

turns eastward to cross the SCS as an undercurrent at depths centered on 200–300 m [*Shaw and Chao*, 1994]. This Southeast Vietnam Offshore Current is associated with the dipole structure of SSHa persistently observed in September and October between 11° and 14°N in the western basin (Figure 11e) [*Ho et al.*, 2000; *Shaw et al.*, 1999]. Given that these latitudes correspond to the entrance into the Sulu Sea via Mindoro Strait, it may be that this subsurface eastward jet is the source of the southward intermediate flow observed over the same 200–300 m depth range in these passages during this fall transition. As the NEM progresses, the stronger positive wind stress curl results in a basin-wide cyclonic gyre with anomalously high SSHa around the perimeter of the SCS (Figure 11f) that strengthens the southward western boundary current [*Shaw and Chao*, 1994; *Wu et al.*, 1998]. While some of this current contributes to the higher throughflow into Karimata Strait during the NEM [*Qu et al.*, 2005; *Fang et al.*, 2010], the high SSH along the northeast coast of Borneo (Figures 11f and 12) suggests that some of this flow continues eastward. The continuity of high sea level through both Balabac Strait into the western part of the Sulu Sea, as well as along the Palawan island chain into Mindoro Strait, suggests there may be further partitioning of this flow through both channels (Figure 12). Unfortunately there are no direct current observations in the vicinity of Balabac Strait as yet to confirm this circulation pattern, although the sea level (through geostrophy) and model results offer some support [e.g., *Shaw and Chao*, 1994]. Thus it appears likely that the cyclonic gyre circulation within the SCS during the NEM results in the strong intermediate depth southward flow observed through Mindoro and Panay Straits, although what causes the shoaling of the southward flow from the fall transition to the NEM is less certain. In their model, *Wang et al.* [2003] suggest that during the dynamic adjustment to long westward Rossby waves excited at the eastern boundary of the SCS during the monsoon reversals result in the propagation of coastally trapped Kelvin waves around the perimeter of the SCS. The shoaling of the southward flow may possibly be a signal of the upward phase propagation of these waves leaking into the Sulu Sea. The pulse-like nature of the southward flow may be related to surges in the wind field within the SCS or perhaps time-variations in the pressure head that drives the flow from the western Pacific through Luzon Strait [*Metzger and Hurlburt*, 1996]. Targeted model experiments are required to help further diagnose the suspected controlling forces.

[42] The isolated northward transport reversals evident in February–March 2008 and again in mid-May 2008 also have the characteristic upward phase propagation associated with Kelvin waves. In this case it is likely that the Rossby wave energy from the western Pacific Ocean boundary has been converted into coastal Kelvin wave energy that propagates around the Philippine archipelago. Saltier water was associated with northward flow at 312-m depth in Mindoro Strait (Figure 3a) and at this depth, northward flow only occurs during the isolated events in February–March and May 2008 (Figure 8a). The saltier water is sourced from intermediate depths in the Sulu Sea [*Quadfasel et al.*, 1990; *Tessler et al.*, 2010] supporting the notion of upward phase propagation as the Kelvin wave passes along the eastern Sulu Sea. In the BRAN data-assimilating model, *Liu et al.* [2011] tracked Kelvin wave signals northward along the waveguide of the eastern edge of the Sulu Sea through Panay and Mindoro Straits to reach the northern tip of Luzon Island. Kelvin wave pathways into the Sulu Sea from the Pacific can be either via Sibutu Passage from the Sulawesi Sea, or directly through Dipolog or San Bernardino Straits (Figure 1). All these straits, as well as the three straits measured as part of this study have passage widths much smaller than the mean baroclinic Rossby deformation radius which ranges from 100 to 150 km at these latitudes [*Chelton et al.*, 1998]. The propagation pathways, frequency of the Kelvin wave events and their relationship to Pacific forcing are the subject of future analysis.

5.3. The Benthic Layer

[43] Bottom intensified flows are evident in both Mindoro and Panay Straits. Earlier studies suggested that these benthic overflows might be episodic turbidity currents related to cyclone activity in the SCS [*Quadfasel et al.*, 1990; *Gamo et al.*, 2007], although more recent analysis demonstrated the transport is hydraulically controlled, at least in Panay Strait [*Tessler et al.*, 2010]. In this paper, bottom temperature time series showed substantial variability over the deployment period, with a range of >2°C in Mindoro Strait and ~0.5°C in Panay and Tablas Strait. The stronger variability in the Mindoro Strait bottom temperature may be a function of the seasonal change in thermocline depth of the SCS that shoals and upwells colder water during the NEM with the reverse occurring during the SWM. On the same isopycnal, *Tessler et al.* [2010] showed that SCS T-S properties, the source of the NPIW overflow in Mindoro, were cooler and fresher than those observed on the sill in Panay Strait. Thus, even though the sill depth is shallower at Mindoro (~440 m) compared to Panay (~560 m), the coolest temperature observed at Mindoro was >0.5°C cooler than the coldest temperature recorded in the Panay time series (Figure 4). This was particularly the case during episodes of stronger southward flow. While at Tablas (with a similar sill depth to

Panay), the sill temperatures were typically 0.5°C warmer than at Panay. This suggests that the cooler (and fresher) Mindoro Strait overflow waters mix within the Semirara Sea with the much warmer (and saltier) waters exiting over the deeper sill in Tablas Strait before overflowing Panay Strait. This supports the idea that mixing and warming of the cooler SCS overflow water occurs relatively quickly after water plunges over the sills [*Tessler et al.*, 2010].

6. Conclusions

[44] The mean annual transports from the SCS into the Sulu Sea during 2008 were very small, of O(0.1) Sv, even though individual transport events of O(1) Sv were observed in all depth layers and could occur at any time of the year. Our best transport estimates give −0.07 (±1.11) Sv in Mindoro Strait and −0.03 (±0.36) Sv in Tablas Strait with −0.44 (±0.77) Sv exiting through Panay Strait. It is clear that although the variability is strong, there is little balance in the total transports during our 2008 survey year. Based on the discussion above, the discrepancy appears mainly due the stronger southward transport in Panay Strait at intermediate depth during the NEM (Figure 10b) and in the benthic transport during the fall transition (Figure 10c). These discrepancies may be due to the sub-optimal position of the Mindoro mooring east of the main channel not capturing the strongest southward flow in both layers. While the extrapolated transport for the missing Tablas observations at depth generally agrees with the Panay-Mindoro residual transport (Figure 10c), thus supporting a small benthic contribution from Tablas, it is likely that there is significant deep southward benthic flow occurring through Tablas Strait in fall.

[45] The PhilEx mooring deployment period in 2008 coincided with a reasonably strong La Niña that peaked during February–March 2008, so it is reasonable to ask how "typical" are these transport estimates. The high-resolution modeling study by *Hurlburt et al.* [2011] showed stronger southward flow through Mindoro Strait during 2004, an El Niño year, compared to 2008. The main difference between the 2004 and 2008 Mindoro Strait model transports appears to be the lack of northward transport in the surface layer during the SWM, but rather in 2004 the annual cycle is dominated by the stronger southward flows such as characterize the NEM in 2008. The model and observed annual mean SSHa during 2004 (2008) is anomalously low (high) throughout the SCS and Sulu Sea (Figure 11) (see also Figure 3 of *Hurlburt et al.* [2011]). Thus it may be that the mechanisms suggested above as responsible for the observed northward flow during the 2008 SWM – regional wind-eddy processes in the Sulu Sea and the summer anticyclonic gyre set-up in the central SCS – are enhanced during La Niña years, and conversely, much diminished during El Niño years. Various studies suggest there is stronger Luzon Strait transport and weaker Kuroshio transport during El Niño years as a result of the northward shift of the NEC bifurcation [*Masumoto and Yamagata*, 1991; *Yaremchuk and Qu*, 2004; *Qu et al.*, 2004; *Qiu and Chen*, 2010]. The situation is reversed during La Niña years. Thus it appears likely that the relatively weak transports observed to enter the Sulu Sea from the SCS during the 2008 mooring deployment are a result of the coincident strong La Niña event.

[46] **Acknowledgments.** A large part of the success of PhilEx is due to the skill and dedication of the Captain and crew of the R/V *Melville* and the many U.S. and Philippine students, technicians, and scientists who participated and assisted in the fieldwork. We also thank Phil Mele for the processing of the L-ADCP data. The research was supported by the Office of Naval Research grants N00014-06-1-690 to Scripps Institution of Oceanography, U.C. San Diego, N00014-09-1-0807 to the University of Hawai'i, and N00014-09-1-0582 to Lamont-Doherty Earth Observatory of Columbia University. This is contribution 8548 from the School of Ocean and Earth Sciences and Technology, University of Hawai'i and Lamont-Doherty Earth Observatory contribution 7536.

References

Becker, J. J., et al. (2009), Global bathymetry and elevation data at 30-arc seconds resolution: SRTM30_PLUS, *Mar. Geod.*, *32*(4), 355–371, doi:10.1080/01490410903297766.

Cai, S., Y. He, S. Wang, and X. Long (2009), Seasonal upper circulation in the Sulu Sea from satellite altimetry data and a numerical model, *J. Geophys. Res.*, *114*, C03026, doi:10.1029/2008JC005109.

Centurioni, L. R., P. P. Niiler, and D. K. Lee (2004), Observations of inflow of Philippine Sea surface water in to the South China Sea through Luzon Strait, *J. Phys. Oceanogr.*, *34*, 113–121, doi:10.1175/1520-0485(2004)034<0113:OOIOPS>2.0.CO;2.

Chelton, D. B., R. A. deSzoeke, M. G. Schlax, K. El Naggar, and N. Siwertz (1998), Geographical variability of the first-baroclinic Rossby radius of deformation, *J. Phys. Oceanogr.*, *28*, 433–460, doi:10.1175/1520-0485(1998)028<0433:GVOTFB>2.0.CO;2.

Chen, C.-T. A., E.-P. Hou, T. Gamo, and S. L. Wang (2006), Carbonate related parameters of subsurface waters in the west Philippine, South China and Sulu Seas, *Mar. Chem.*, *99*, 151–161, doi:10.1016/j.marchem.2005.05.008.

Fang, G., R. D. Susanto, I. Soesilo, Q. Zheng, F. Qiao, and Z. Wei (2005), A note on the South China Sea shallow interocean circulation, *Adv. Atmos. Sci.*, *22*, 946–954.

Fang, G., Y. Wang, Z. Wei, Y. Fang, F. Qiao, and X. Hu (2009), Interocean circulation and heat and freshwater budgets of the South China Sea based on a numerical model, *Dyn. Atmos. Oceans*, *47*(1–3), 55–72, doi:10.1016/j.dynatmoce.2008.09.003.

Fang, G., R. D. Susanto, S. Wirasantosa, F. Qiao, A. Supangat, B. Fan, Z. Wei, B. Sulistiyo, and S. Li (2010), Volume, heat, and freshwater transports from the South China Sea to Indonesian seas in the boreal winter of 2007–2008, *J. Geophys. Res.*, *115*, C12020, doi:10.1029/2010JC006225.

Gamo, T., Y. Kato, H. Hasumoto, H. Kakiuchi, N. Momoshima, N. Takahata, and Y. Sano (2007), Geochemical implications for the mechanism of deep convection in a semi-closed tropical marginal basin: Sulu Sea, *Deep Sea Res.*, *54*, 4–13, doi:10.1016/j.dsr2.2006.06.004.

Gordon, A. L., and C. L. Villanoy (2011), The oceanography of the Philippine archipelago: Introduction to the Special Issue, *Oceanography*, *24*(1), 13, doi:10.5670/oceanog.2011.13.

Gordon, A. L., J. Sprintall, and A. Ffield (2011), Regional oceanography of the Philippine archipelago, *Oceanography*, *24*(1), 14–27, doi:10.5670/oceanog.2011.01.

Han, W., A. M. Moore, E. Di Lorenzo, A. L. Gordon, and J. Lin (2008), Seasonal surface ocean circulation and dynamics in the Philippine archipelago region during 2004–2008, *Dyn. Atmos. Oceans*, *47*, 114–137.

Ho, C.-R., Q. Zheng, Y. S. Soong, N.-J. Kuo, and J.-H. Hu (2000), Seasonal variability of sea surface height in the South China Sea observed with Topex/Poseidon altimeter data, *J. Geophys. Res.*, *105*, 13,981–13,990, doi:10.1029/2000JC900001.

Hurlburt, H., J. Metzger, J. Sprintall, S. N. Riedlinger, R. A. Arnone, T. Shinoda, and X. Xu (2011), Circulation in the Philippine archipelago simulated by 1/12° and 1/25° global HYCOM and EAS NCOM, *Oceanography*, *24*(1), 28–47, doi:10.5670/oceanog.2011.02.

Jones, B. H., C. M. Lee, G. Toro-Farmer, E. S. Boss, M. C. Gregg, and C. L. Villanoy (2011), Tidally driven exchange in an archipelago strait: Biological and optical responses, *Oceanography*, *24*(1), 142–155, doi:10.5670/oceanog.2011.11.

Lebedev, K. V., and M. I. Yaremchuk (2000), A diagnostic study of the Indonesian Throughflow, *J. Geophys. Res.*, *105*, 11,243–11,258, doi:10.1029/2000JC900015.

Lermusiaux, P. F. J., P. J. Haley Jr., W. G. Leslie, A. Agarwal, O. G. Logutov, and L. J. Burton (2011), Multiscale physical and biological dynamics in the Philippine archipelago: Predictions and processes, *Oceanography*, *24*(1), 70–89, doi:10.5670/oceanog.2011.05.

Liu, Q., M. Feng, and D. Wang (2011), ENSO-induced interannual variability in the southeastern South China Sea, *J. Oceanogr.*, *67*, 127–133, doi:10.1007/s10872-011-0002-y.

Logutov, O. G. (2008), A multi-grid methodology for assimilation of measurements into regional tidal models, *Ocean Dyn.*, *58*, 441–460, doi:10.1007/s10236-008-0163-4.

Masumoto, Y., and T. Yamagata (1991), Response of the western tropical Pacific to the Asian winter monsoon: The generation of the Mindanao Dome, *J. Phys. Oceanogr.*, *21*, 1386–1398, doi:10.1175/1520-0485(1991)021<1386:ROTWTP>2.0.CO;2.

May, P. W., J. D. Doyle, J. D. Pullen, and L. T. David (2011), Two-way coupled atmosphere-ocean modeling of the PhilEx intensive observational periods, *Oceanography*, *24*(1), 48–57, doi:10.5670/oceanog.2011.03.

McClean, J. L., D. P. Ivanova, and J. Sprintall (2005), Interannual variability of the Indonesian Throughflow from WOCE IX1 XBT data and a global eddy-permitting ocean model, *J. Geophys. Res.*, *110*, C10013, doi:10.1029/2004JC002477.

Metzger, E. J., and H. E. Hurlburt (1996), Coupled dynamics of the South China Sea, the Sulu Sea, and the Pacific Ocean, *J. Geophys. Res.*, *101*, 12,331–12,352, doi:10.1029/95JC03861.

Ohlmann, J. C. (2011), Drifter observations of small-scale flows in the Philippine archipelago, *Oceanography*, *24*(1), 122–129, doi:10.5670/oceanog.2011.09.

Pullen, J., J. D. Doyle, P. May, C. Chavanne, P. Flament, and R. A. Arnone (2008), Monsoon surges trigger oceanic eddy formation and propagation in the lee of the Philippine Islands, *Geophys. Res. Lett.*, *35*, L07604, doi:10.1029/2007GL033109.

Pullen, J. D., A. L. Gordon, J. Sprintall, C. M. Lee, M. H. Alford, J. D. Doyle, and P. W. May (2011), Atmospheric and oceanic processes in the vicinity of an island strait, *Oceanography*, *24*(1), 112–121, doi:10.5670/oceanog.2011.08.

Qiu, B., and S. Chen (2010), Interannual to decadal variability in the bifurcation of the North Equatorial Current off the Philippines, *J. Phys. Oceanogr.*, *40*, 2525–2538, doi:10.1175/2010JPO4462.1.

Qu, T. (2000), Upper-layer circulation in the South China Sea, *J. Phys. Oceanogr.*, *30*, 1450–1460, doi:10.1175/1520-0485(2000)030<1450:ULCITS>2.0.CO;2.

Qu, T., and Y. T. Song (2009), Mindoro Strait and Sibutu Passage transports estimated from satellite data, *Geophys. Res. Lett.*, *36*, L09601, doi:10.1029/2009GL037314.

Qu, T., H. Mitsudera, and T. Yamagata (2000), Intrusions of the North Pacific waters into the South China Sea, *J. Geophys. Res.*, *105*, 6415–6424, doi:10.1029/1999JC900323.

Qu, T., Y. Y. Kim, M. Yaremchuk, T. Tozuka, A. Ishida, and T. Yamagata (2004), Can the Luzon Strait transport play a role in conveying the impact of ENSO to the South China Sea?, *J. Clim.*, *17*, 3644–3657, doi:10.1175/1520-0442(2004)017<3644:CLSTPA>2.0.CO;2.

Qu, T., Y. Du, G. Meyers, A. Ishida, and D. Wang (2005), Connecting the tropical Pacific with Indian Ocean through the South China Sea, *Geophys. Res. Lett.*, *32*, L24609, doi:10.1029/2005GL024698.

Qu, T., Y. Du, and H. Sasaki (2006), South China Sea throughflow: A heat and freshwater conveyor, *Geophys. Res. Lett.*, *33*, L23617, doi:10.1029/2006GL028350.

Quadfasel, D., H. Kudrass, and A. Frische (1990), Deep-water renewal by turbidity currents in the Sulu Sea, *Nature*, *348*, 320–322, doi:10.1038/348320a0.

Shaw, P. T., and S. Y. Chao (1994), Surface circulation in the South China Sea, *Deep Sea Res.*, *41*, 1663–1683, doi:10.1016/0967-0637(94)90067-1.

Shaw, P. T., S. Y. Chao, and L. L. Fu (1999), Sea surface height variations in the South China Sea from satellite altimetry, *Oceanol. Acta*, *22*, 1–17, doi:10.1016/S0399-1784(99)80028-0.

Sprintall, J., S. E. Wijffels, R. Molcard, and I. Jaya (2009), Direct estimates of the Indonesian Throughflow entering the Indian Ocean, *J. Geophys. Res.*, *114*, C07001, doi:10.1029/2008JC005257.

Takeda S., N. Ramaiah, M. Miki, Y. Kondo, Y. Yamaguchi. Y. Arii, F. Gomez, K. Furuya, and W. Takahashi (2007), Biological and chemical characteristics of the high-chlorophyll, low-temperature water observed near the Sulu archipelago, *Deep Sea Res.*, *54*(1–2), 81–102, doi:10.1016/j.dsr2.2006.08.020.

Tessler, Z., A. L. Gordon, L. Pratt, and J. Sprintall (2010), Panay Sill overflow dynamics, *J. Phys. Oceanogr.*, *40*, 2679–2695, doi:10.1175/2010JPO4395.1.

Wang, D., W. Wang, P. Shi, P. Guo, and Z. Gan (2003), Establishment and adjustment of monsoon-driven circulation in the South China Sea, *Sci. China Ser. D*, *46*(2), 173–181, doi:10.1360/03yd9016.

Wang, G., D. Chen, and J. Su (2008), Winter eddy genesis in the eastern South China Sea due to orographic wind jets, *J. Phys. Oceanogr.*, *38*, 726–732, doi:10.1175/2007JPO3868.1.

White, W. B., Y. M. Tourre, M. Barlow, and M. Dettinger (2003), A delayed action oscillator shared by biennial, interannual, and decadal signals in the Pacific Basin, *J. Geophys. Res.*, *108*(C3), 3070, doi:10.1029/2002JC001490.

Wu, C.-R., P.-T. Shaw, and S.-Y. Chao (1998), Seasonal and interannual variations in the velocity field of the South China Sea, *J. Oceanogr.*, *54*, 361–372, doi:10.1007/BF02742620.

Wyrtki, K. (1961), *Physical Oceanography of the Southeast Asian Waters*, *Naga Rep. 2*, 195 pp., Scripps Inst. Oceanogr, La Jolla, Calif.

Yaremchuk, M., and T. Qu (2004), Seasonal variability of the large-scale currents near the coast of the Philippines, *J. Phys. Oceanogr.*, *34*, 844–855, doi:10.1175/1520-0485(2004)034<0844:SVOTLC>2.0.CO;2.

Yaremchuk, M., J. L. McCreary, Z. J. Yu, and R. Furue (2009), The South China Sea throughflow retrieved from climatological data, *J. Phys. Oceanogr.*, *39*, 753–767, doi:10.1175/2008JPO3955.1.

Yu, Z., J. P. McCreary, M. Yaremchuk, and R. Furue (2008), Subsurface salinity balance in the South China Sea, *J. Phys. Oceanogr.*, *38*, 527–539, doi:10.1175/2007JPO3661.1.